Beta cell dysfunction and dedifferentiation induced by Bone Morphogenetic Protein (BMP)-2 is associated with histone modifications and decreased NeuroD1 chromatin binding

Adriana Ibarra
https://orcid.org/0000-0003-3672-1910
Michala Prause
University of Copenhagen
Lars Ingerslev
University of Copenhagen
Matthew Wortham
University of California, San Diego
Yinghui Sui
University of California, San Diego
Maike Sander
UCSD
Kristine Williams
University of Copenhagen
Romain Barrès
University of Copenhagen
Martin Larsen
Gitte Christensen
University of Copenhagen
Nils Billestrup (billestrup@sund.ku.dk)
University of Copenhagen

Article

Keywords:

Posted Date: November 23rd, 2022

DOI: https://doi.org/10.21203/rs.3.rs-2254065/v1

Version of Record: A version of this preprint was published at Cell Death & Disease on July 5th, 2023. See the published version at https://doi.org/10.1038/s41419-023-05906-w.

Abstract

Insufficient insulin secretion is a hallmark of type 2 diabetes and has been attributed to beta cell identity loss characterized by decreased expression of several key beta cell genes. The pro-inflammatory factor BMP-2 is upregulated in islets of Langerhans from individuals with diabetes and acts as an inhibitor of beta cell function and proliferation. Exposure to BMP-2 induces expression of *Id1-4*, *Hes-1* and *Hey-1* which are transcriptional regulators associated with loss of differentiation.

The aim of this study was to investigate the mechanism by which BMP-2 induces beta cell dysfunction and loss of cell maturity. Mouse islets exposed to BMP-2 for 10 days showed impaired glucose-stimulated insulin secretion and beta cell proliferation. BMP-2-induced beta cell dysfunction was associated with decreased expression of cell maturity and proliferation markers specific to the beta cell such as *Ins1*, *Ucn3* and *Ki67* and increased expression of *Id1-4*, *Hes-1* and *Hey-1*. Top 30 most regulated proteins significantly correlated with corresponding mRNA expression. BMP-2-induced gene expression changes were associated with a predominant reduction in acetylation of H3K27 and a decrease in NeuroD1 chromatin binding activity.

These results show that BMP-2 induces loss of beta cell maturity and suggest that remodeling of H3K27ac and decreased NeuroD1 DNA binding activity participate in the effect of BMP-2 on beta-cell dysfunction.

Introduction

Type 2 diabetes mellitus (T2D) is characterized by relative insulin deficiency caused by insulin resistance and beta cell dysfunction. The observed progressive deterioration of beta cell mass and function in T2D has traditionally been associated with apoptosis (1, 2). However, dedifferentiation of beta cells towards less mature and dysfunctional cells has been suggested as an alternative explanation for the loss of insulin-positive cell mass in T2D (3). In mouse models of T2D, beta cell dedifferentiation and loss of beta cell identity have been associated with decreased expression of several transcription factors that are crucial for the maintenance of beta cell function, including FoxO1 (3), Nkx6.1 (4) and NeuroD1 (5, 6). This has also been described in some studies of human islets (6, 7), although there is considerable heterogeneity of T2D islet datasets, with the extent of beta cell identity marker repression being dependent on methodology and patient cohort (8, 9). Moreover, hyperglycemia, inflammation and oxidative stress are all factors associated with T2D, and thought to alter the expression of these beta cell specific transcription factors (3, 10–12) and thus contribute to beta cell dedifferentiation.

Bone Morphogenetic Proteins (BMPs) are members of the TGF-β family of growth and differentiation factors and are known to play central roles in pancreas and islet development (13, 14). Moreover, emerging data points to BMPs, particularly BMP-2 and − 4, as inflammatory factors, which are also associated with obesity, T2D and beta cell dysfunction (15–19). mRNA expression of *BMP-2* and − *4* is upregulated in pancreatic islets of *db/db* mice, and *BMP-2* expression is induced by pro-inflammatory

cytokines in rodent and human islets *in vitro* (18, 20, 21). In human islets, the expression of *BMP-2* is correlated positively with donor HbA1c, suggesting a potential role in beta cell dysfunction (22, 23). Further, BMP-2 and − 4 have been described to act as potent inhibitors of beta cell proliferation and function *in vitro* in both rodent and human islets (18, 24).

BMP-2 and − 4 bind to the BMP type I receptor, activin-like kinase (ALK)-3 and − 6, and forms a complex with the BMP type II receptors. This receptor complex stimulates the activation of SMAD1/5/8 and subsequently the expression of inhibitory basic helix-loop-helix (bHLH) factors, such as the four Inhibitor of DNA binding proteins (Id1-4), Hairy and enhancer of split-1 (Hes-1), and Hairy/enhancer-of-split related with YRPW motif protein 1 (Hey-1) (25, 26). The Id proteins as well as Hey-1 and Hes-1, are known to inhibit the transcriptional activity of other central beta cell bHLH factors, including NeuroD1, (25, 27, 28) and are known to inhibit differentiated cell function in many cells types (29, 30). Specifically in beta cells, both Id and Hes-1 expression are associated with poor beta cell function and dedifferentiation (31–33).

Epigenetic modifications play a central role in cellular differentiation and maintenance of cellular identity and disruption of epigenetic modifications can have pathophysiological consequences (34). Histone modifications have been shown to be involved in beta cell differentiation, identity, function and proliferation (35–38). Moreover, evidence suggests that epigenetic mechanisms may be involved in the pathogenesis of diabetes (38–41). Polycomb dependent histone methylation events have been implicated in beta cell dedifferentiation in both mouse and human beta cell dysfunction resulting in increased expression of genes associated with immature beta cell phenotype and a decrease in expression of genes associated with mature beta cells (38). BMPs induce chromatin remodeling in several tissues such as osteoblasts and fibroblast by recruiting or inducing the expression histone modifying enzymes (42, 43). Furthermore, Hes-1 and Hey-1 recruit histone deacetylases (44, 45). Thus, BMPs are likely to induce epigenetic changes that regulate cell differentiation either directly through SMADs or through their downstream targets such as the Id's, Hes-1 and Hey-1.

It has been suggested that loss of beta cell identity occurs in islets of patients with T2D. However, the molecular mechanism of this reprogramming to less mature beta cells has not been elucidated in detail. In the present study we investigate the role of BMP-2 in this process by applying a multi-omics approach (transcriptome, proteome and epigenome) aimed at elucidating BMP-2 effects. BMP-2 is produced locally by islets when exposed to inflammation (21) and increased BMP-2 serum concentrations have been found in T2D patients (19, 23). We hypothesize that prolonged exposure of pancreatic islets to BMP-2 results in epigenetic alterations affecting the expression of key beta cell genes leading to loss of beta cell maturity and dysfunction.

Results

BMP-2 induces beta cell dysfunction and inhibition of proliferation

In order to study the effects of long-term BMP-2 exposure on beta cell function and proliferation, primary mouse islets were isolated and cultured *in vitro* for 10 days in the presence or absence of BMP-2 (50 ng/mL). Exposure of islets to BMP-2 for 10 days resulted in a significant reduction of glucose-stimulated insulin secretion (GSIS) (Fig. 1A) without significantly affecting total islet insulin content (Fig. 1B).

Next, we examined whether BMP-2 affected beta cell proliferation in cultures of intact mouse islets. Proliferating beta cells were identified by EdU incorporation into Pdx-1 positive cells. After 10 days, control islets showed 1.8% Pdx-1 positive cells whereas no beta cell proliferation was observed after BMP-2 exposure (Fig. 1C and D). To determine whether the inhibition of GSIS and proliferation by BMP-2 was associated with apoptosis, we analyzed islet cell apoptosis. Exposure of islets to BMP-2 for 10 days did not induce islet cell apoptosis, whereas increased release of cytoplasmic nucleosomes, as a measurement for induction of apoptosis, was observed in islets exposed to a cytokine combination of IL-1β (300 pg/ml) and IFN-γ (10 ng/ml) for 48 hours (Fig. 1E).

Bmp-2 Induces Changes In Markers Of Beta Cell Maturity

We hypothesize that BMP-2-induced beta cell dysfunction is associated with changes in expression of beta cell maturity genes and genes involved in cell proliferation. Total RNA was isolated from islets exposed to BMP-2 for 10 days or left non-exposed and selected beta cell specific gene expression were analyzed by qRT-PCR.

BMP-2 significantly reduced expression of *Ins1* and *Ucn3* mRNA's in mouse islets compared to control islets (Fig. 2A). No significant differences were observed in mRNA expression of *Ins2*, *MafA* or *Pdx1*, whereas *Glp1r* expression was significantly upregulated ~ 2-fold by BMP-2 exposure. The proliferation markers *Ki67* and *Cdk1* were significantly reduced by BMP-2 to nearly non-detectable levels (Fig. 2B) supporting the observation of BMP-2-inhibited beta cell proliferation.

Expression of known BMP-2 target genes was also analyzed. BMP-2 exposure for 10 days significantly induced *Hes-1* expression by ~ 3.5-fold (Fig. 2A) and *Hey-1* mRNA expression by ~ 60-fold in primary mouse islets (Fig. 2C).

The transition towards a less mature and dysfunctional beta cell requires changes in the transcription factor network regulating multiple genes. To characterize transcriptional effects of BMP-2 exposure more globally, we performed mRNA-sequencing (mRNA-seq). Comparison of gene expression profiles of mouse islets exposed to BMP-2 or left non-exposed, showed significant differences in the expression of 1580 genes (FDR < 0.05 and FC > 1.5), of which 612 were upregulated and 968 were downregulated by BMP-2 (Figs. 3A and B).

Consistent with the qRT-PCR data, the expression of *Ucn3* was significantly reduced by BMP-2 as was expression of the proliferation markers *Ki67*, *Top2a*, and *Cdk*1 by 71, 51 and 34-fold respectively (Fig. 3A, Suppl. datasheet 1). Expression of well-known BMP-2 signaling pathway targets such as *Id1*, *Calb1* and

Hey-1 were upregulated (Fig. 3A, Suppl.1). In order to identify biological pathways affected by BMP-2 we performed Gene ontology (GO) analysis on the differentially expressed genes. BMP-2 upregulated genes were enriched in biological process pathways involved in insulin and peptide transport and secretion pathways and monocarboxylic acid and lipid metabolic processes (Fig. 3C, Suppl. datasheet 2). Of interest, upregulation of the negative regulators of insulin secretion *Ucp2* (46, 47) and *Acvr1c* (48) could explain the decreased insulin secretion capacity observed in BMP-2 exposed islets. BMP-2 downregulated genes were strongly associated with functional pathways of cell cycle, replication and cell division (Fig. 3D, Suppl. datasheet 3).

Bmp-2 Regulated Gene Expression Correlates With Protein Expression

Next, we investigated whether BMP-2 regulated mRNA expression correlated with protein expression. A global proteomic analysis was performed on mouse islets exposed to BMP-2 or left non-exposed for 10 days. BMP-2 exposure led to significant up- and downregulation of 211 and 131 proteins, respectively (protein > 2 peptides, Adj. P-value > 0.05, FC > 0.3) (Fig. 4A, Suppl. Figure 1, Suppl. datasheet 4 and 5). A top 35 most up- or downregulated proteins list was generated with corresponding mRNA expression (Table 1). We found a significant correlation between BMP-2 protein product and mRNA expression (Fig. 4B). In accordance with the mRNA-seq data, CALB1 protein level was significantly upregulated by BMP-2 while glucagon was downregulated. No significant changes were observed in INS1, MAFA and PDX1 protein expression after BMP-2 stimulation. GO analysis showed that only one biological process pathway upregulated upon BMP-2 stimulation, *the regulation of system processes* (Suppl. datasheet 6) and one downregulated protein pathway related to *endoplasmic reticulum (ER) stress* (Suppl. datasheet 7). Of importance, we did also observe a significant GO term related to ER stress at mRNA level (Suppl. datasheet 3). A STRING analysis on BMP-2 downregulated proteins (FC > 0.5) further revealed highly confident networks of protein processing in ER and signal peptide processing. Interestingly, and supporting our GO analysis on cell cycle, protein networks associated to DNA replication minichromosome maintenance protein complex (MCM) important for cell division and various checkpoint pathways were also identified (Suppl. Figure 2).

Bmp-2 Regulates Histone Modifications

We next investigated whether changes in gene expression induced by BMP-2 were associated with histone modifications. We analyzed three specific modifications, H3K27ac, H3K4me3, and H3K27me3 by chromatin immunoprecipitation followed by sequencing (ChIP-seq) using chromatin preparations from isolated islets cultured in the absence or presence of BMP-2 for 10 days. Of the three modifications analyzed, we found H3K27ac to be the most affected by BMP-2 where a total of 13611 regulated peaks (FDR Poisson P value < 0.0001 and FC > 2) were identified with 13179 peaks found to be enriched in the control (down by BMP-2) and 432 peaks were found to be enriched in the BMP-2 exposed conditions (Fig. 5A and D). For H3K4me3, a total of 662 regulated peaks (FC > 2) were identified with 213 peaks

enriched in the control and 449 peaks increased by BMP-2 exposure (Fig. 5B and D). For H3K27me3, a total of 91 peaks were regulated with 60 and 31 peaks (FC > 2) found to be enriched in the control or BMP-2 exposed cells, respectively (Fig. 5C-D) (List of differential peaks, Suppl. datasheet 8–13).

We hypothesized that BMP-2 exposure leads to a reduction of H3K27ac near transcription start site (TSS) of mature beta cell genes, leading to decreased transcription. We found that the beta cell marker *Ucn3* as well as the proliferation markers *MKi67* and *Top2a* had lower levels of H3K27 acetylation in the proximity to their respective TSS while the BMP-2 enhanced genes *Id1* and *Hey-1* showed increased H3K27ac marks at the TSS (Fig. 5E). This is in agreement with the mRNA expression data. Furthermore, an increase in H3K4 tri-methylation was found in vicinity of the genes encoding *Id1* (Fig. 5E).

As H3K27ac and H3K4me3 were the histone modifications found to be most strongly affected by BMP-2, we next analyzed the link between differentially regulated histone signals (H3K27ac and H3K4me3 associated to TSS of annotated genes) and mRNA expression (Fig. 6A-D). Downregulation of mRNA expression was significantly correlated with a decrease in H3K27ac in control enriched peaks (Fig. 6A) while an upregulation of mRNA expression by BMP-2 was significantly correlated with an increase in H3K27ac (Fig. 6C). A similar correlation was found for H3K4me3; a decrease in mRNA expression was significantly correlated with a decrease in H3K4me3 (Fig. 6B) while an increase in gene expression by BMP-2 was significantly correlated with an increase in H3K4me3 (Fig. 6D). Accordingly, genes proximal to differential H3K27ac or H3K4me3 sites following BMP-2 treatment exhibited concordant changes in mRNA levels, with the exception of sites losing H3K4me3 (Suppl. Figure 3A-D). We further performed GO analysis of genes with significantly regulated peaks in their promoters. Several significant GO Biological processes were identified in H3K27ac downregulated peaks all of which related to proliferation and cell cycle regulation and organization (Fig. 6E, Suppl. datasheet 15). H3K27ac upregulated peaks by BMP-2 were associated to GO terms related to BMP response and signaling and differentiation of various cell types (Fig. 6F, Suppl. datasheet 14). No Biological Processes GO terms were significant for H3K4me3 peak associated genes (Suppl. datasheet 16 and 17).

Bmp-2 Stimulation Leads To A Decrease In Neurod1 Binding To Chromatin

Motif analysis (HOMER) of H3K27ac peaks revealed NeuroD1 and other bHLH family members binding sites within H3K27ac peaks downregulated by BMP-2 (Fig. 7A). No statistically significant motifs were found in BMP-2 regulated H3K4me3 peaks. Since Id proteins are known to dimerize with other bHLH factors such as NeuroD1, preventing their binding to DNA, we analyzed if the decrease in H3K27ac peaks was associated with a decrease in NeuroD1 binding. NeuroD1 ChIP analysis showed that BMP-2 reduced NeuroD1 binding to chromatin. A total of 11053 NeuroD1 binding sites were identified, of those, 2412 binding sites showed a significant change (FDR Poisson P-value < 0.0001, FC > 2) upon BMP-2 exposure. Of these 2336 peaks showed decreased binding and only 76 peaks showed increased binding following BMP-2 exposure (Fig. 7B). As expected, NeuroD1 was found to bind in the promotors of key beta cell

genes such as *Ins1/2* and *Pdx1*. However, no significant differences in the binding to these specific sites were observed between control and BMP-2 exposed islets. Instead, we found a significant reduction of NeuroD1 binding in the promotors of the beta cell markers *MafA*, *Ucn3* and *FoxO1* (a list of differential peaks can be found in Suppl. datasheet 18 and 19). Comparison of the distribution of NeuroD1 binding sites in the genome demonstrated that differently occupied sites were depleted of promoters and enriched in intergenic and intronic regions in response to BMP-2 (Fig. 7C). Biological Processes GO analysis revealed that BMP-2 downregulated NeuroD1 binding was enriched in gene sets of organismal processes, development and signaling (Fig. 7D, Suppl. datasheet 20).

Discussion

In this study we have explored the changes in function, gene and protein expression, and histone modifications in mouse islets exposed to BMP-2, to better understand the mechanism behind BMP-2-induced beta cell dysfunction.

Beta pancreatic cells exposed to BMP-2 showed decreased insulin release in response to glucose, which was associated with a marked reduction in mRNA expression of genes controlling beta cell function such as *Ins1* and *Ucn3* and upregulation of Calbindin1 (*Calb1*). We have previously showed that BMP-4-induced increase in *CALB1* expression is associated with impaired insulin secretion (24). Changes in *Ins1* expression did not translate into decreased insulin protein expression, when analyzed by proteomics or ELISA from islet extracts. However, and in contrast to the insulin expression data, our top 35 protein expression analysis on BMP-2 exposed mouse islets showed significant correlation between regulation of mRNA and protein expression.

The BMP-2 induced beta cell dysfunction was also associated with an increased expression of the bHLH family members *Id1-3*, *Hey-1* and *Hes-1* which are negative regulators of bHLH transcription factor activity (25, 27). The Notch signaling pathway is known to induce Hes-1 activation, but is largely inactive in adult pancreas tissue. However, under certain conditions associated with dedifferentiation (e.g., *in vitro* culture and cytokine exposure) Notch signaling can be re-activated (32, 49). The upregulation of Hes-1 in cultured human islets was associated with an increase in beta cell proliferation and dedifferentiation (32). Moreover, inhibition of insulin expression by Hes-1 has been suggested to be due to Hes-1 direct binding to NeuroD1 or Pdx1 thus decreasing *Ins* gene transcription (33, 49). However, increase in *Hes-1* mRNA in this study was not associated with an increase in proliferation.

Beta cell proliferation was significantly reduced by BMP-2 exposure. Top 10 gene ontology of biological processes downregulated by BMP-2 showed an enrichment of genes associated with cell proliferation, cell cycle division and chromosome segregation, indicating that BMP-2 might exert its effects on proliferation by inhibiting the progression of G2/M phase. Of interest, we found decreased expression of *Cdk1*, *Ki67*, *Cenpf* and *Top2a*, which are markers of replicating beta cells (50). Further, STRING analysis of BMP-2 downregulated proteins revealed decreased expression of several proteins in the MCM complex critical for DNA replication (51) and glucose-induced proliferation (52). G1/S CDK complexes play a

crucial role in beta cell proliferation in mouse and human, and loss of either CDK4 or Cyclin D2 leads to a dramatic loss of beta cell mass and proliferation, resulting in diabetes (53, 54). CDK6 alone or in combination with a D-Cyclin can drive human beta-cell replication *in vitro* and *in vivo* (55, 56). Furthermore, nutrients and growth factors have been shown to induce beta cell replication by inducing the progression of G1/S (57, 58). In this study, we have not found differences in the mRNA or protein expression of *Cdk4*, *Cdk6* nor *Ccnd2*. However, reduced mRNA expression of *Ccnd1* was observed. CCND1 forms a complex with CDK4, E2F1 and E2F2, which are both activators of the G1/S transition and significantly reduced by BMP-2. In addition, overexpression of Hes-1 has been shown to arrest the human breast T47D cells in the G1 phase of the cell cycle by repressing the expression of *E2F1* (59). Altogether, this data suggests that BMP-2 inhibits proliferation by inhibiting the progression of G1/S and G2/M phase.

Epigenetic regulation is essential for proper function including cell proliferation. We analyzed the BMP-2-induced changes in three histone marks known to affect chromatin structure and gene transcription in islet cells. The observed reduction in H3K27ac mark following BMP-2 exposure and the association with cell cycle genes (e.g., *Top2a*, *Mki67* and *E2f2*) suggest that this histone modification is significant and plays a role in the inhibition of beta cell proliferation induced by BMP-2. In agreement with RNA-seq data, *Gcg* and *Ucn3* also show reduced H3K27ac in the proximity to their TSS, while *Pdx1* showed an increase. Furthermore, *Pdx1* and *Glp1r* contained an increase in the H3K4me3 mark. Both H3K27ac and H3K4me3 marks have previously been found to be associated with several beta cell specific genes in human and mouse islets, indicating that they might play an important role in the regulation of transcription of these genes (60–62).

Motif analysis of BMP-2 downregulated H3K27ac peaks revealed enrichment in NeuroD1 binding sites and other bHLH family members. NeuroD1 ChIP-seq confirmed that BMP-2 stimulated cells had a decreased NeuroD1 binding to chromatin. Both the Id proteins and Hes-1/Hey-1 inhibit the transcriptional activity of bHLH factors. The Id proteins, which lack a DNA binding domain, dimerize with bHLH transcription factors such as NeuroD1 to prevent their binding to DNA and thereby reduce transcription (25). On the other hand, Hes-1 and Hey-1 bind E- and N- box sequences as homo- or heterodimers and act as transcriptional repressors. Hes-1/Hey-1 can also form dimers with bHLH transcription factors and change the transactivating activity to repression while maintaining DNA binding activity (63). The fact that BMP-2 stimulation caused a general decrease in NeuroD1 chromatin binding without affecting the NeuroD1 mRNA level or protein expression suggests a model in which Id proteins prevent NeuroD1 binding by forming Id/NeuroD1 dimers. However, a role for Hes-1/Hey-1 to heterodimerize with NeuroD1 and subsequent recruitment of transcriptional repressors could also be at play. Further analysis of the Id and Hes-1/Hey-1 binding partners in BMP-2 stimulated islets is required to characterize the mechanism in more detail. Hey-1 proteins have been shown to directly interact with the co-repressors N-CoR and mSin3A, which in turn are able to recruit histone deacetylase-1 (HDAC1) and induce gene silencing (44). Hes-1 has also been described to recruit another histone deacetylase, SIRT1 (45). We speculate that the recruitment of co-repressor by Hes-1/Hey-1 might induce the observed reduction on H3K27ac upon BMP-2 exposure.

In conclusion, in this study we show that prolonged exposure to BMP-2 is associated with beta cell dysfunction and inhibition of proliferation. We provide evidence that BMP-2 exposure leads to a reduction in H3K27ac, which is associated with reduced expression of positive regulators of the cell cycle. BMP-2 exposure was also associated with a decrease in NeuroD1 binding, indicating that Id proteins might be the effectors of beta cell dysfunction induced by BMP-2.

Methods And Materials

Mouse islet isolation and culture

Pancreata from 12 week old male C57BL/6NJR mice (Janvier, Saint Berthewin Cedex, France) or 12 week old male C57BL/6NTAC mice (Taconic, Lille Skensved, Denmark) were inflated with Liberase (Roche, Hvidovre, Denmark), excised and incubated at 37 Cº to allow digestion. Digestion was halted by adding Hanks' balanced salt solution (HBSS; Lonza, Basel, Switzerland) supplemented with bovine serum albumin (BSA; Sigma, Soeborg, Denmark). Islets were handpicked and cultured for 1 day in 10 ml RPMI 1640 medium (Lonza) with 11mmol/l D-Glucose supplemented with 10% fetal bovine serum (FBS; Biosera, Herlev, Denmark) and 1% penicillin/streptomycin (100 U/ml penicillin, 100 µg/ml streptomycin) (P/S; Gibco, Life Technologies, Roskilde, Denmark). Thereafter islets were cultured for 10 days at 37 Cº in a humidified atmosphere with 5% CO^2 in 10 ml RPMI 1640, 2% human serum (HS; Lonza) and 1% P/S in the absence or presence of 50 ng/ml recombinant human BMP-2 (R&D Systems, Life Technologies). Medium was changed every fifth day. For GSIS, apoptosis and proliferation analysis, islets from individual mice were used. For RNA isolation, Proteomic and ChIP-seq analysis, pools of islets from several mice were used. All animal experiments were approved by the local ethics committee, and animals were housed according to the Principals of Laboratory Care.

Glucose-stimulated Insulin Release And Insulin Content

GSIS was performed with 25 islets per condition in biological duplicates as previously described (64). In brief, islets were pre-cultured for 1.5h in Krebs-Ringer HEPES buffer (KRHB; 115 mmol/l, NaCl, 4.7 mmol/l KCl, 2.6 mmol/l CaCl2, 1.2 mmol/l KH2PO4, 1.2 mmol/l MgSO4, 10 mmol/l HEPES, 0.2% BSA, 2 mmol/l glutamine, 5 mmol/l NaHCO3 and 1% penicillin and streptomycin, pH 7.4) with 2 mM D-glucose followed by 30 min of incubation in KRHB with 2 mM D-glucose and then 30 min of incubation in KRBH with 20 mM D-glucose. The buffer was then collected from each experimental group and insulin content was determined using an in-house ELISA. Results were corrected for DNA content using Quant-IT PicoGreen dsDNA Reagent and Kit (Life Technologies).

Proliferation

Beta cell proliferation was analyzed in intact mouse islets cultured on extracellular matrix coated slides (Biological Industries, Israel). 10 uM EdU (ethynyl-2'-deoxyuridine) (Life Technologies) was given 24 h

prior fixation in 1% PFA. Proliferating beta cells were detected with Click-iT EdU Proliferatio n Assay (Life Technologies), followed by staining of pancreatic duodenal homeobox 1 (Goat-anti Pdx1; 1:5000, ab2027, Beta cell biology consortium) and Hoechst (#3342, Life Technologies). Islet cells positive for both Pdx1 and EdU were counted as proliferating beta cells. Whole islets were examined by capturing z-stack images using Zeiss Axio Obsever Z1 with spinning disk (Zeiss, Birkerød, Denmark) and counted using the ZEN software (Zeiss). A minimum of 700 cells were examined per experiment in each condition. For representation, a median filter with binding 2x2 pixels was applied (Image J).

Cell Death Detection Assay

Apoptotic cell death was measured in 25 islets per condition in duplicates by the detection of DNA histone complexes released from the nucleus to the cytosol using Cell Death Detection ELIS APLUS (Roche) as described by the manufacturer. As a positive control for apoptosis mouse islets were exposed for 48 h to 300 pg/ml recombinant mouse IL-1β (cat. 554577, BD Biosciences, Lyngby, Denmark) combined with 10ng/ml IFN-γ (cat. 585-IF, R&D System, Life Technologies). To adjust for differences in cell number among different conditions, islet lysates were sonicated and DNA was quantified by Quant-IT PicoGreen dsDNA Reagent and Kit (Life technologies).

Gene Expression Analysis

A total of 200–400 intact mouse islets were cultured as described and lysed in Trizol. Total mRNA purification was performed using Direct-zol RNA-mini prep kit according to the manufacturer's protocol (Zymo Research, Nordic Biosite, Copenhagen, Denmark). cDNA was synthesized by qScript cDNA Super mix kit (Quanta Biosciences, Beverly, MA, USA). Quantitative expression levels of mRNA of interest were evaluated using Taqman Gene Expression probes and performed on a ABI PRISM 7900HT Sequence Detection system (Applied Biosystems, Nærum, Denmark). Each sample was measured in triplicates and expression was normalized to the internal control, Ppia. The TaqMan Gene Expression probes against Ins1 (Mm01950294_s1), Ins2 (Mm00731595_gh), Mafa (Rn00845206_s1), Ucn3 (Mm00453208), Pdx1 (Mm00435565), Glp1R (00445292_m1), Hes-1 (Rn00577566_m1), Hey-1 (Rn00448865_m1), Ki67 (Mm01278617_m1), Cdk1 (Mm00772472-m1) and Ppia (Rn00690933_m1) were used for quantifying mRNA expression of the different genes.

Rna-seq

RNA was isolated from 500 islets per condition (N = 3) using the RNeasy® Micro Kit (Qiagen) according to the manufacturer instructions. For RNA sequencing (RNA-seq), stranded, single-end sequencing libraries were constructed from 35 ng of isolated RNA using the TruSeq® Stranded mRNA Library Prep Kit (Cat# 20020595, Illumina®, San Diego, CA, USA). Library sequencing was performed on a HiSeq 4000 System (Illumina®). Both library construction and sequencing were performed by the IGM core research facility at University of California San Diego, USA.

Single-end 50 bp RNA-seq reads were mapped to the UCSC mouse genome (mm9) by STAR v. 2.4.0 (–outSAMstrandField intronMotif –outFilterMultimapNmax 1 –rethread 5), allowing for up to 10 mismatches (default by STAR) (65). Only the reads aligned uniquely to one genomic location were retained for subsequent analysis. Expression levels of all genes were estimated by Cufflinks v2.2.1 (-p 6 -G $gtf_file –max-bundle-frags 1000000000) (66) using only the reads with exact matches. Differential gene expression was performed using Cuffdiff (Cufflinks v2.2.1), with FDR < 0.05 considered significant.

RNA-seq data from control islets are identical to the data set published previously as these samples served as controls for both BMP-2 stimulation (this study) and IL-1ß stimulation (67). This was done in an effort to comply with the 3R principles for animal research.

To identify the functional categories of differential expressed genes, GO analysis of Biological Processes was performed using the enrichGO function from the R package clusterProfiler v. 4.4.4 (68) using the org.Mm.eg.db v 3.15.0 database (69) with all expressed genes as the universe (background) and genes with a FDR less than 0.05 as significant genes (foreground), only terms containing between 10 and 500 expressed genes were analyzed. GO analysis was performed separately for genes that were up- or downregulated. Dot-plots were generated using the dotplot function, which is part of clusterProfiler. Color was mapped to –log10 (P-value) instead of raw P-value. Ontologies with a FDR less than 0.05 was considered significant and the top 10 most significant terms were visualized in the dot-plots. Suppl. Tables of ontologies includes non-significant ontologies with a more lenient FDR cutoff of 0.5.

Proteomics

150 intact mouse islets per condition (N = 5) were collected and washed x3 in Phosphate-buffered saline (PBS). Islets for the proteomics workflow were lysed, reduced and pre-digested in 10 µl lysis buffer (6 M Urea, 2 M Thiourea, 10 mM DTT) (Sigma) and 1 µg Lys-C (Wako) supplemented with PhosSTOP phosphatase inhibitor (Roche) for 2 h at RT. Then lysates were diluted 10 times using 20 mM Triethylammonium bicarbonate buffer (TEAB; pH 8) and tip-sonicated for 2x10 sec on ice at 60% amplitude. Then, samples were alkylated by 20 mM Iodacetamide for 20 min in the dark before digestion with 2% (w/w) trypsin (Sigma) overnight (ON) at 30°C.

A total of 100 µg tryptic peptides from each sample were labeled with TMT10 plex according to the manufactures protocol (Controls: TMT126-TMT128C; BMP-2: TMT129N-TMT131). After labeling, the samples were mixed in 1:1 ratio and the sample was dried by vacuum centrifugation. The lyophilized sample was re-solubilized in 0.1% TFA and an aliquot corresponding to 100 µg peptide was desalted using a micro Oligo R3 (Applied Biosystems) Reversed phase column as described previously (70). The desalted peptide sample was dried by vacuum centrifugation.

Hydrophilic interaction liquid chromatography (HILIC)

The peptide samples were subjected to fractionation using HILIC. Briefly, these samples were resuspended in 90% ACN, 0.1% TFA (Solvent B) and loaded onto a 450 µM OD x 320 µM ID x 17 cm micro-capillary column packed with TSK Amide-80 resin material (Tosoh Bioscience) using an Agilent 1200 Series HPLC (Agilent). Peptides were separated using a gradient from 100 – 60% Solvent B (Solvent A: 0.1% TFA) running for 30 min at a flow-rate of 6 µL/min. Fractions were collected every 1 min and combined into 13 final fractions based on the UV chromatogram and subsequently dried by vacuum centrifugation.

Reversed-phase nanoLC-ESI-MS/MS

The samples were re-suspended in 0.1% TFA and loaded onto an EASY-nLC system (Thermo Scientific). The samples were loaded onto a two-column system containing a 3 cm pre-column and a 17 cm analytic column both consisting of fused silica capillary (75 µm inner diameter) packed with ReproSil – Pur C18 AQ 3 µm reversed-phase material (Dr. Maisch). The peptides were loaded onto the pre-column in buffer A (0.1% Formic acid (FA)). The peptides were eluted with an organic solvent gradient from 1% buffer B (95% ACN, 0.1% FA) to 7% buffer B at a constant flow rate of 250 nl/min for 3 min and then up to 28% buffer B for 55 min, up to 40% buffer B in 3 min and finally to 95% buffer B in 3 min. The nanoLC was online connected to an Orbitrap Fusion Lumos (Thermo Fisher Scientific) operated at positive ion mode with data-dependent acquisition. The Lumos acquired the full MS scan with an automatic gain control (AGC) target value of 1x106 ions and a maximum fill time of 50ms. Each MS scan was acquired at high-resolution (120,000 full width half maximum (FWHM)) at m/z 200 in the Orbitrap with a mass range of 400–1600 Da. The Lumos was set to one full MS per 3 s to allow for maximum amount of precursor ions to be selected for fragmentation in these 3 s. The most abundant peptide ions were selected from the MS for higher energy collision-induced dissociation (HCD) fragmentation (normalized collision energy: 40V). Fragmentation was performed at high resolution (50,000 FWHM) for a target of 1x105 and a maximum injection time of 100 ms using an isolation window of 1.2 m/z and a dynamic exclusion of 20 sec. All raw data were viewed in Xcalibur v3.0 (Thermo Fisher Scientific).

MS data processing and statistical analysis

All LC-MSMS raw data files were searched using Proteome Discoverer version 2.1. The raw data were searched in PD using a workflow where the raw data were first subjected to database searching using an in-house Mascot server (Version 2.2.04, Matrix Science Ltd., London, UK) and then the spectra that did not yield a high confident identification was further searched using Sequest HT. The searches had the following criteria: database, SwissProt mouse protein database (updated 2017-10) for the Mascot search and uniprot mouse (version 17.07.2017; 75193 sequences) for the Sequest HT search; enzyme, trypsin; maximum missed cleavages, 2; fixed modifications, TMT6plex (N-terminal), TMT6plex (K) and Carbamidomethyl (C). The TMT10 plex reporter ion signals were quantified using S/N and they were normalized to the total S/N in the PD program. After database search the protein with normalized abundances were extracted and the proteins with 2 or more identified peptides were used for further analysis. The statistic significant regulated proteins were selected using the program Perseus (71) using

multiple sample testing (ANOVA), Benjamini-Hochberg Adj. P value (> 0.05%), FC (> 0.3). Perseus was also used for generation of PCA plots, heat maps and cluster analysis. GO was performed as with RNA-seq data, using all proteins with 2 or more identified peptides as foreground and proteins with a FDR less than 0.1 as significant. The analysis was performed on up- and downregulated proteins separately.

Histone Modification Chip-seq

1200–1500 mouse islets per condition (N = 3) were cross-linked for 10 min with 1.11% formaldehyde, quenched with 0.125 M glycine, lysed in 1% SDS and sheared with a BioRuptor Sonicator (Diagenode, Denville, NJ, USA) for 8 cycles of 5 min. ChIP was performed according to the manufacturer's instructions (ChIP-IT High Sensitivity, cat# 53040, Active Motif, Carlsbad, CA, USA) using 10–30 µg of sonicated chromatin and the following antibodies for immunoprecipitation: H3K4 trimethylation (Cat#04-745, Millipore, Burlington, MA, USA) H3K27 acetylation (Cat#39133, Active Motif) or H3K27 trimethylation (Cat# 07-449, Millipore). Immune complexes were captured with 60µl of 50% protein G sepharose beads, washed and eluted in TE buffer. DNA fragments were purified using the ChIP-IT sensitivity kit filter columns. ChIP-seq libraries were prepared using KAPA DNA Library Preparation Kits for Illumina® (Cat# KK8234, Kapa Biosystems, Boston, MA, USA) and the library sequencing was performed on the HiSeq 4000 System (Illumina®).

Library construction and sequencing were performed by the Institute for Genomic Medicine (IGM) core research facility at UCSD. All histone modification ChIP-seq data was mapped to the UCSC mouse genome NCBI37/mm9 (July 2007). Bowtie 2 was used to map data to the genome with the following settings: the seed length was set as 33 with a maximum number of 2 mismatches allowed in the seed region, and reads aligning to multiple locations were discarded. After mapping, duplicate reads were removed using Samtools. ChIP-seq data from control islets are identical to the data set published previously as these samples served as controls for both BMP-2 stimulation (this study) and IL-1ß stimulation (67).

Histone Modification Chip-seq Analysis

Two replicates per condition were combined. The chromatin used for immunoprecipitation was likewise sequenced and used to normalize for differences in input. ChIP-seq analysis was performed using HOMER (Hypergeometic Otimization of Motif EnRichment). Peak calling. Peaks were required to have a 2-fold enrichment over the input sample (default setting by HOMER) and Poisson P value of < 0.0000001. For H3K27ac and H3K4me3 "factor mode" was run. To account the broader signal of H3K27me3 "–region –size 1000 –minDist 1000 –tagThreshold 50 mode" was run for peak calling. Differential Peak calling. Peaks that were differentially enriched between control and BMP-2 were identified using the getDifferentialPeaks command in HOMER. Peaks were required to have 2-fold enrichment between experimental groups (FDR Poisson P value of 0.0001). Gene annotation. Peaks were associated with the nearest gene, and the position of the TSS was determined using the annotatePeaks.pl command in

HOMER, All parameters were left at their default setting. Motif Finding. Enriched motifs in ChIP-Seq peaks were identified using findMotifsGenome.pl using the -bg option to correct for background enrichment. Background was generated by removing enriched peaks from the full list of peaks in each sample using bedtools. All parameters were left at their default setting. Heat maps. Heat maps of differential peaks were generated using the annotatePeaks.pl function in HOMER. Tag densities within 50 bp bins spanning 6000 bp around the peak center were used to generate heat map data. Rows were sorted decreasingly by the sum of the tag density in the center 2000 bp, and heat maps were generated using the heatmap.2 function of the gplots package in R. RNA-seq heat maps were also generated using the heatmap.2 function of the gplots package in R. If expression=="up" & significant==“yes”, the color is red; if expression==“down" & significant=="yes”, the color is green; others are blue.

Genes with peaks overlapping selected for gene ontology analysis. Gene ontology analysis of genes with significantly differentially enriched ChIP-seq peaks was performed and visualized as described in the RNA-seq section. All genes with a detected peak overlapping a region 3000 bp upstream to 1000 bp downstream of their TSS were used as background and genes where the overlapping peak(s) were significantly differentially enriched, as defined above, were used as foreground, only terms containing between 10 and 500 genes with peaks were analyzed. The analysis was performed on genes with up- and downregulated peaks separately.

Neurod1 Chip-seq

1200 islets per condition (N = 2) were cross-linked for 10 min in 1.11% formaldehyde, lysed in ice-cold IP buffer (67 mM Tris-HCl (pH 8), 100 mM NaCl, 5 mM EDTA (pH 8.0), 0.2% NaN_3, 0.33% SDS, 1,67% Triton X-100, 0.5 mM phenylmethylsulfonyl fluoride) and sonicated (Diagenode, BioRuptor) for 45 cycles of alternating 30 s intervals of sonication and rest. For each ChIP, chromatin corresponding to 1.4–1.6 µg of DNA was incubated overnight at 4 Cº with NeuroD1 antibody (Cat#4373, Cell Signaling). Immune complexes were captured by incubation with protein G sepharose beads (GE healthcare) for 4 h. The beads were washed three times with low-salt buffer (20 mM Tris-HCl (pH 8.0), 2 mM EDTA (pH 8.0), 1% Triton X-100, 0.1% SDS, 150 mM NaCl) and one time with high-salt buffer (20 mM Tris-HCl (pH 8.0), 2 mM EDTA (pH 8.0), 1% Triton X-100, 0.1% SDS, 500 mM NaCl). Chromatin was de-cross-linked in 120 µl 1% SDS and 0.1M NaHCO3 for 6 h at 65 Cº, and DNA fragments were purified using Quiagen MinElute PCR purification kit filter columns. Finally, ChIP-seq libraries were prepared using NEBNext® UltraTM DNA library Kit for Illumina® (E7370) and NEBNext® Multiplex Oligos for Illumina® (E7335/E7500). The PCR cycle number for each library amplification was optimized by running 10% of the library DNA in a real-time PCR reaction using Brilliant III Ultra-fast SYBR Green QPCR Master Mix (AH Diagnostic) and a C1000 Thermal cycler (Bio-Rad). DNA libraries were sequenced on a NextSeq 500 (Illumina®) by 38-bp paired-end sequencing.

Neurod1 ChIP-seq data was mapped to the UCSC mouse genome NCBI37/mm10. Bowtie 2 was used to map data to the genome with the following settings: the seed length was set as 33 with a maximum

number of 2 mismatches allowed in the seed region, and reads aligning to multiple locations were discarded. After mapping, duplicate reads were removed using samtools.

Neurod1 Chip-seq Analysis

Two replicas per condition were combined. The chromatin used for immunoprecipitation was likewise sequenced and used to normalize for differences in input. ChIP-seq analysis was performed using HOMER (Hypergeometic Otimization of Motif EnRichment). Peak calling. Peaks were required to have 2-fold enrichment over the input sample (default setting by HOMER) and Poisson P value of < 0.0000001 and “-style factor” was run for peak calling.

Gene ontology analysis of NeuroD1 binding sites was performed using the Genomic Regions Enrichment of Annotations Tool (GREAT) v. 4.0.4 (72) on 2022-05-05 using default settings. All detected Neuro-D1 binding sites were used as background and significantly differentially enriched binding sites, as defined above, were used as foreground. The analysis was run separately for sites with increased and decreased binding. A dot-plot similar to the one generated for RNA-seq was manually constructed using the R package ggplot2 (73). The top 10 terms with a FDR less than 0.05 were visualized. On the x-axis is the percentage of genes that are within 1000 kb of at least one differentially enriched binding site out of all genes in the term that are within 1000 kb of at least one binding site, the size of the dot corresponds to the number of genes with one or more differentially enriched binding sites within 1000kb. The color is mapped to −log10 (P-value) as reported by GREAT.

Statistical analysis

Results are given as mean (N < 10) or mean ± SD (N > 10). Comparison versus the respective control group was made by Student’s 2-tailed paired t-test and a P-value less than 0.05 was considered statistically significant. Statistics on RT-qPCR data was carried out using log-transformed data. For RNA and ChIP-seq correlation analysis, nonparametric Spearman correlation was used. Differentially expressed genes were identified with Cuffdiff using a statistical cutoff of FDR < 0.05. ChIP-seq peaks exhibiting differential signal between treatment groups were identified using the getDifferentialPeaks command in HOMER (cutoff of 2-fold enrichment between groups and FDR Poisson P-value of 0.0001).

Declarations

Acknowledgments

We thank Helle Fjordvang, Faculty of Health and Medical Sciences, University of Copenhagen for her expert technical assistance. Further, we acknowledge the Core Facility for Integrated Microscopy (CFIM), Faculty of Health and Medical Sciences, University of Copenhagen. We acknowledge support of the UCSD IGM Genomic Center (supported by P30 DK064391) for library preparation and sequencing. We

acknowledge the Single-Cell Omics platform at the Novo Nordisk Foundation Center for Basic Metabolic Research (CBMR) for technical and computational expertise and support.

Conflict of Interest Statement

The authors have no conflict of interest.

Author Contribution Statement

AI, MP, MW, GLC, NB conceived and designed the study. AI, MP, GLC, KW, MRL performed the experiments. AI, MP, LRI, YS, MW, MS, KW, RB, MRL, GLC and NB performed analysis and interpretation of data. AI, LRI, YS, MW, MRL performed bioinformatics and statistical analysis. AI, MP, GLC and NB contributed to writing the first manuscript draft. All the authors read, reviewed and approved the final version of the manuscript.

Ethics Statement

Animal studies were performed according to the regulations of the institutional animal care and use committee of the University of Copenhagen (authorization number P 18-416)

Funding Statement

This work was supported by Novo Nordisk Foundation through the Danish Diabetes Academy (G.L.C and M.P), European Foundation for the Study of Diabetes (Program in cellular plasticity underlying the pathophysiology of type 2 diabetes), Augustinus Fonden (G.L.C), Juvenile Diabetes Research Foundation grant 3-PDF-2014- 193-A-N (M.W), U.S. Department of Health & Human Services | NIH | National Institute of Diabetes and Digestive and Kidney Diseases grant R01 DK068471 and R01 DK078803 (M.S), VILLUM Center for Bioanalytical Sciences (VILLUM Foundation grant no. 7292), by PRO-MS, Danish National Mass Spectrometry Platform for Functional Proteomics (grant no. 5072-00007B).

Data Availability

Supplementary information is available at Cell Death and Differentiation's website.

Proteomics data are available via ProteomeXchange with identifier PXD036655.

For review; reviewer_pxd036655@ebi.ac.uk, **Password:** sjqtuZSk

RNAseq and ChIP-seq data are available at the GEO repository, GSE216233 with the reviewer token: ytalekagndirloz.

References

1. Butler AE, Janson J, Bonner-Weir S, Ritzel R, Rizza RA, Butler PC. Beta-cell deficit and increased beta-cell apoptosis in humans with type 2 diabetes. Diabetes. 2003;52(1):102-10.
2. Tsai S, Clemente-Casares X, Revelo XS, Winer S, Winer DA. Are obesity-related insulin resistance and type 2 diabetes autoimmune diseases? Diabetes. 2015;64(6):1886-97.
3. Talchai C, Xuan S, Lin HV, Sussel L, Accili D. Pancreatic beta cell dedifferentiation as a mechanism of diabetic beta cell failure. Cell. 2012;150(6):1223-34.
4. Taylor BL, Liu FF, Sander M. Nkx6.1 is essential for maintaining the functional state of pancreatic beta cells. Cell Rep. 2013;4(6):1262-75.
5. Gu C, Stein GH, Pan N, Goebbels S, Hornberg H, Nave KA, et al. Pancreatic beta cells require NeuroD to achieve and maintain functional maturity. Cell Metab. 2010;11(4):298-310.
6. Dominguez V, Raimondi C, Somanath S, Bugliani M, Loder MK, Edling CE, et al. Class II phosphoinositide 3-kinase regulates exocytosis of insulin granules in pancreatic beta cells. J Biol Chem. 2011;286(6):4216-25.
7. Avrahami D, Wang YJ, Schug J, Feleke E, Gao L, Liu C, et al. Single-cell transcriptomics of human islet ontogeny defines the molecular basis of beta-cell dedifferentiation in T2D. Mol Metab. 2020;42:101057.
8. Mawla AM, Huising MO. Navigating the Depths and Avoiding the Shallows of Pancreatic Islet Cell Transcriptomes. Diabetes. 2019;68(7):1380-93.
9. Gloyn AL, Ibberson M, Marchetti P, Powers AC, Rorsman P, Sander M, et al. Every islet matters: improving the impact of human islet research. Nat Metab. 2022;4(8):970-7.
10. Guo S, Dai C, Guo M, Taylor B, Harmon JS, Sander M, et al. Inactivation of specific beta cell transcription factors in type 2 diabetes. J Clin Invest. 2013;123(8):3305-16.
11. Kjorholt C, Akerfeldt MC, Biden TJ, Laybutt DR. Chronic hyperglycemia, independent of plasma lipid levels, is sufficient for the loss of beta-cell differentiation and secretory function in the db/db mouse model of diabetes. Diabetes. 2005;54(9):2755-63.
12. Nordmann TM, Dror E, Schulze F, Traub S, Berishvili E, Barbieux C, et al. The Role of Inflammation in beta-cell Dedifferentiation. Sci Rep. 2017;7(1):6285.
13. Ahnfelt-Ronne J, Ravassard P, Pardanaud-Glavieux C, Scharfmann R, Serup P. Mesenchymal bone morphogenetic protein signaling is required for normal pancreas development. Diabetes. 2010;59(8):1948-56.
14. Wagner DO, Sieber C, Bhushan R, Borgermann JH, Graf D, Knaus P. BMPs: from bone to body morphogenetic proteins. Sci Signal. 2010;3(107):mr1.
15. Ribeiro S, Lopes LR, Paula Costa G, Figueiredo VP, Shrestha D, Batista AP, et al. CXCL-16, IL-17, and bone morphogenetic protein 2 (BMP-2) are associated with overweight and obesity conditions in middle-aged and elderly women. Immun Ageing. 2017;14:6.
16. Bostrom KI, Jumabay M, Matveyenko A, Nicholas SB, Yao Y. Activation of vascular bone morphogenetic protein signaling in diabetes mellitus. Circ Res. 2011;108(4):446-57.

17. Bottcher Y, Unbehauen H, Kloting N, Ruschke K, Korner A, Schleinitz D, et al. Adipose tissue expression and genetic variants of the bone morphogenetic protein receptor 1A gene (BMPR1A) are associated with human obesity. Diabetes. 2009;58(9):2119-28.
18. Bruun C, Christensen GL, Jacobsen ML, Kanstrup MB, Jensen PR, Fjordvang H, et al. Inhibition of beta cell growth and function by bone morphogenetic proteins. Diabetologia. 2014;57(12):2546-54.
19. Guiu-Jurado E, Unthan M, Bohler N, Kern M, Landgraf K, Dietrich A, et al. Bone morphogenetic protein 2 (BMP2) may contribute to partition of energy storage into visceral and subcutaneous fat depots. Obesity (Silver Spring). 2016;24(10):2092-100.
20. Eizirik DL, Sammeth M, Bouckenooghe T, Bottu G, Sisino G, Igoillo-Esteve M, et al. The human pancreatic islet transcriptome: expression of candidate genes for type 1 diabetes and the impact of pro-inflammatory cytokines. PLoS Genet. 2012;8(3):e1002552.
21. Ibarra Urizar A, Friberg J, Christensen DP, Lund Christensen G, Billestrup N. Inflammatory Cytokines Stimulate Bone Morphogenetic Protein-2 Expression and Release from Pancreatic Beta Cells. J Interferon Cytokine Res. 2016;36(1):20-9.
22. Fadista J, Vikman P, Laakso EO, Mollet IG, Esguerra JL, Taneera J, et al. Global genomic and transcriptomic analysis of human pancreatic islets reveals novel genes influencing glucose metabolism. Proc Natl Acad Sci U S A. 2014;111(38):13924-9.
23. Zhang M, Sara JD, Wang FL, Liu LP, Su LX, Zhe J, et al. Increased plasma BMP-2 levels are associated with atherosclerosis burden and coronary calcification in type 2 diabetic patients. Cardiovasc Diabetol. 2015;14:64.
24. Christensen GL, Jacobsen ML, Wendt A, Mollet IG, Friberg J, Frederiksen KS, et al. Bone morphogenetic protein 4 inhibits insulin secretion from rodent beta cells through regulation of calbindin1 expression and reduced voltage-dependent calcium currents. Diabetologia. 2015;58(6):1282-90.
25. Benezra R, Davis RL, Lockshon D, Turner DL, Weintraub H. The protein Id: a negative regulator of helix-loop-helix DNA binding proteins. Cell. 1990;61(1):49-59.
26. Miyazono K, Miyazawa K. Id: a target of BMP signaling. Sci STKE. 2002;2002(151):pe40.
27. Iso T, Kedes L, Hamamori Y. HES and HERP families: multiple effectors of the Notch signaling pathway. J Cell Physiol. 2003;194(3):237-55.
28. Jensen J, Pedersen EE, Galante P, Hald J, Heller RS, Ishibashi M, et al. Control of endodermal endocrine development by Hes-1. Nat Genet. 2000;24(1):36-44.
29. Norton JD. ID helix-loop-helix proteins in cell growth, differentiation and tumorigenesis. J Cell Sci. 2000;113 (Pt 22):3897-905.
30. Weber D, Wiese C, Gessler M. Hey bHLH transcription factors. Curr Top Dev Biol. 2014;110:285-315.
31. Akerfeldt MC, Laybutt DR. Inhibition of Id1 augments insulin secretion and protects against high-fat diet-induced glucose intolerance. Diabetes. 2011;60(10):2506-14.

32. Bar Y, Russ HA, Knoller S, Ouziel-Yahalom L, Efrat S. HES-1 is involved in adaptation of adult human beta-cells to proliferation in vitro. Diabetes. 2008;57(9):2413-20.
33. Shinozuka Y, Okada M, Oki T, Sagane K, Mizui Y, Tanaka I, et al. Altered expression of HES-1, BETA2/NeuroD, and PDX-1 is involved in impaired insulin synthesis induced by glucocorticoids in HIT-T15 cells. Biochem Biophys Res Commun. 2001;287(1):229-35.
34. Kim JK, Samaranayake M, Pradhan S. Epigenetic mechanisms in mammals. Cell Mol Life Sci. 2009;66(4):596-612.
35. Andrali SS, Sampley ML, Vanderford NL, Ozcan S. Glucose regulation of insulin gene expression in pancreatic beta-cells. Biochem J. 2008;415(1):1-10.
36. Bramswig NC, Everett LJ, Schug J, Dorrell C, Liu C, Luo Y, et al. Epigenomic plasticity enables human pancreatic alpha to beta cell reprogramming. J Clin Invest. 2013;123(3):1275-84.
37. Chen H, Gu X, Su IH, Bottino R, Contreras JL, Tarakhovsky A, et al. Polycomb protein Ezh2 regulates pancreatic beta-cell Ink4a/Arf expression and regeneration in diabetes mellitus. Genes Dev. 2009;23(8):975-85.
38. Lu TT, Heyne S, Dror E, Casas E, Leonhardt L, Boenke T, et al. The Polycomb-Dependent Epigenome Controls beta Cell Dysfunction, Dedifferentiation, and Diabetes. Cell Metab. 2018;27(6):1294-308 e7.
39. Park JH, Stoffers DA, Nicholls RD, Simmons RA. Development of type 2 diabetes following intrauterine growth retardation in rats is associated with progressive epigenetic silencing of Pdx1. J Clin Invest. 2008;118(6):2316-24.
40. Remsberg JR, Ediger BN, Ho WY, Damle M, Li Z, Teng C, et al. Deletion of histone deacetylase 3 in adult beta cells improves glucose tolerance via increased insulin secretion. Mol Metab. 2017;6(1):30-7.
41. Varghese SS, Dhawan S. Polycomb Repressive Complexes: Shaping Pancreatic Beta-Cell Destiny in Development and Metabolic Disease. Front Cell Dev Biol. 2022;10:868592.
42. Pan Q, Wu Y, Lin T, Yao H, Yang Z, Gao G, et al. Bone morphogenetic protein-2 induces chromatin remodeling and modification at the proximal promoter of Sox9 gene. Biochem Biophys Res Commun. 2009;379(2):356-61.
43. Yang D, Okamura H, Nakashima Y, Haneji T. Histone demethylase Jmjd3 regulates osteoblast differentiation via transcription factors Runx2 and osterix. J Biol Chem. 2013;288(47):33530-41.
44. Iso T, Sartorelli V, Poizat C, Iezzi S, Wu HY, Chung G, et al. HERP, a novel heterodimer partner of HES/E(spl) in Notch signaling. Mol Cell Biol. 2001;21(17):6080-9.
45. Takata T, Ishikawa F. Human Sir2-related protein SIRT1 associates with the bHLH repressors HES1 and HEY2 and is involved in HES1- and HEY2-mediated transcriptional repression. Biochem Biophys Res Commun. 2003;301(1):250-7.
46. Robson-Doucette CA, Sultan S, Allister EM, Wikstrom JD, Koshkin V, Bhattacharjee A, et al. Beta-cell uncoupling protein 2 regulates reactive oxygen species production, which influences both insulin and glucagon secretion. Diabetes. 2011;60(11):2710-9.

47. Zhang CY, Baffy G, Perret P, Krauss S, Peroni O, Grujic D, et al. Uncoupling protein-2 negatively regulates insulin secretion and is a major link between obesity, beta cell dysfunction, and type 2 diabetes. Cell. 2001;105(6):745-55.
48. Bertolino P, Holmberg R, Reissmann E, Andersson O, Berggren PO, Ibanez CF. Activin B receptor ALK7 is a negative regulator of pancreatic beta-cell function. Proc Natl Acad Sci U S A. 2008;105(20):7246-51.
49. Darville MI, Eizirik DL. Notch signaling: a mediator of beta-cell de-differentiation in diabetes? Biochem Biophys Res Commun. 2006;339(4):1063-8.
50. Klochendler A, Caspi I, Corem N, Moran M, Friedlich O, Elgavish S, et al. The Genetic Program of Pancreatic beta-Cell Replication In Vivo. Diabetes. 2016;65(7):2081-93.
51. Parker MW, Botchan MR, Berger JM. Mechanisms and regulation of DNA replication initiation in eukaryotes. Crit Rev Biochem Mol Biol. 2017;52(2):107-44.
52. Schvartz D, Coute Y, Sanchez JC. Quantitative proteomics reveals the link between minichromosome maintenance complex and glucose-induced proliferation of rat pancreatic INS-1E beta-cells. J Proteomics. 2014;108:163-70.
53. Kushner JA, Ciemerych MA, Sicinska E, Wartschow LM, Teta M, Long SY, et al. Cyclins D2 and D1 are essential for postnatal pancreatic beta-cell growth. Mol Cell Biol. 2005;25(9):3752-62.
54. Rane SG, Dubus P, Mettus RV, Galbreath EJ, Boden G, Reddy EP, et al. Loss of Cdk4 expression causes insulin-deficient diabetes and Cdk4 activation results in beta-islet cell hyperplasia. Nat Genet. 1999;22(1):44-52.
55. Fiaschi-Taesch N, Bigatel TA, Sicari B, Takane KK, Salim F, Velazquez-Garcia S, et al. Survey of the human pancreatic beta-cell G1/S proteome reveals a potential therapeutic role for cdk-6 and cyclin D1 in enhancing human beta-cell replication and function in vivo. Diabetes. 2009;58(4):882-93.
56. Fiaschi-Taesch NM, Salim F, Kleinberger J, Troxell R, Cozar-Castellano I, Selk K, et al. Induction of human beta-cell proliferation and engraftment using a single G1/S regulatory molecule, cdk6. Diabetes. 2010;59(8):1926-36.
57. Alonso LC, Yokoe T, Zhang P, Scott DK, Kim SK, O'Donnell CP, et al. Glucose infusion in mice: a new model to induce beta-cell replication. Diabetes. 2007;56(7):1792-801.
58. Song WJ, Schreiber WE, Zhong E, Liu FF, Kornfeld BD, Wondisford FE, et al. Exendin-4 stimulation of cyclin A2 in beta-cell proliferation. Diabetes. 2008;57(9):2371-81.
59. Hartman J, Muller P, Foster JS, Wimalasena J, Gustafsson JA, Strom A. HES-1 inhibits 17beta-estradiol and heregulin-beta1-mediated upregulation of E2F-1. Oncogene. 2004;23(54):8826-33.
60. Pasquali L, Gaulton KJ, Rodriguez-Segui SA, Mularoni L, Miguel-Escalada I, Akerman I, et al. Pancreatic islet enhancer clusters enriched in type 2 diabetes risk-associated variants. Nat Genet. 2014;46(2):136-43.
61. Stitzel ML, Sethupathy P, Pearson DS, Chines PS, Song L, Erdos MR, et al. Global epigenomic analysis of primary human pancreatic islets provides insights into type 2 diabetes susceptibility loci. Cell Metab. 2010;12(5):443-55.

62. Tennant BR, Robertson AG, Kramer M, Li L, Zhang X, Beach M, et al. Identification and analysis of murine pancreatic islet enhancers. Diabetologia. 2013;56(3):542-52.
63. Kobayashi T, Kageyama R. Expression dynamics and functions of Hes factors in development and diseases. Curr Top Dev Biol. 2014;110:263-83.
64. Prause M, Pedersen SS, Tsonkova V, Qiao M, Billestrup N. Butyrate Protects Pancreatic Beta Cells from Cytokine-Induced Dysfunction. Int J Mol Sci. 2021;22(19).
65. Dobin A, Davis CA, Schlesinger F, Drenkow J, Zaleski C, Jha S, et al. STAR: ultrafast universal RNA-seq aligner. Bioinformatics. 2013;29(1):15-21.
66. Trapnell C, Williams BA, Pertea G, Mortazavi A, Kwan G, van Baren MJ, et al. Transcript assembly and quantification by RNA-Seq reveals unannotated transcripts and isoform switching during cell differentiation. Nat Biotechnol. 2010;28(5):511-5.
67. Ibarra Urizar A, Prause M, Wortham M, Sui Y, Thams P, Sander M, et al. Beta-cell dysfunction induced by non-cytotoxic concentrations of Interleukin-1beta is associated with changes in expression of beta-cell maturity genes and associated histone modifications. Mol Cell Endocrinol. 2019;496:110524.
68. Wu T, Hu E, Xu S, Chen M, Guo P, Dai Z, et al. clusterProfiler 4.0: A universal enrichment tool for interpreting omics data. Innovation (Camb). 2021;2(3):100141.
69. Carlson M. org.Mm.eg.db: Genome wide annotation for Mouse. R package version 3.15.0 2019.
70. Zarrineh M, Ashrafian S, Jensen P, Nawrocki A, Ansari AM, Rezadoost H, et al. Comprehensive proteomics and sialiomics of the anti-proliferative activity of safranal on triple negative MDA-MB-231 breast cancer cell lines. J Proteomics. 2022;259:104539.
71. Tyanova S, Temu T, Sinitcyn P, Carlson A, Hein MY, Geiger T, et al. The Perseus computational platform for comprehensive analysis of (prote)omics data. Nat Methods. 2016;13(9):731-40.
72. McLean CY, Bristor D, Hiller M, Clarke SL, Schaar BT, Lowe CB, et al. GREAT improves functional interpretation of cis-regulatory regions. Nat Biotechnol. 2010;28(5):495-501.
73. Wickham H. ggplot2: Elegant Graphics for Data Analysis: Springer-Verlag New York; 2016.

Tables

Table 1 Top 35 most upregulated proteins and corresponding genes by BMP2:

	Gene name	Protein name	Abundance protein Ratio: (BMP2) / (Control)	Abundance protein Ratio Adj. P-Value: (BMP2) / (Control)	Abundance mRNA Ratio: (BMP2) / (Control)	Abundance mRNA Ratio Adj. P-Value: (BMP2) / (Control)
1	Abcg2	Broad substrate specificity ATP-binding cassette transporter ABCG2	7,83	0,000001	19,46	0,000618
2	H1-4	Histone H1.4	5,81	0,005678	N.A	N.A
3	Ca15	Carbonic anhydrase 15	5,10	0,000066	6,49	0,000618
4	Mxra7	Matrix-remodeling-associated protein 7	3,97	0,000062	9,64	0,000618
5	S100a6	Protein S100-A6	3,71	0,019002	3,26	0,013735
6	Rpl14	60S ribosomal protein L14	3,40	0,074282	0,97	0,894231
7	Apoa5	Apolipoprotein A-V	3,29	0,000142	99,64	0,000618
8	Krt20	Keratin, type I cytoskeletal 20	3,11	0,020971	24,75	0,377516
9	Vstm2l	V-set and transmembrane domain-containing protein 2-like protein	3,08	0,007263	1,63	0,000618
10	Dap	Death-associated protein 1	3,00	0,004513	1,12	0,401089
11	Calb1	Calbindin	2,93	0,000001	4,01	0,000618
12	Lsm6	U6 snRNA-associated Sm-like protein LSm6	2,86	0,029078	0,94	0,748914
13	Iqgap2	Ras GTPase-activating-like protein IQGAP2	2,81	0,000003	6,42	0,000618
14	Spock2	Testican-2	2,66	0,000031	2,27	0,000618
15	Rps20	40S ribosomal protein S20	2,61	0,032729	0,87	0,331214
16	H2ac20	Histone H2A type 2-C	2,60	0,016075	N.A	N.A
17	Rpl34	60S ribosomal protein L34	2,59	0,052033	0,95	0,957406

18	Tppp3	Tubulin polymerization-promoting protein family member 3	2,42	0,048060	3,72	0,000618
19	Gsta1	Glutathione S-transferase A1	2,41	0,081305	N.A	N.A
20	Anxa10	Annexin A10	2,37	0,026457	3,55	0,119353
21	Ptgr1	Prostaglandin reductase 1	2,37	0,009449	3,64	0,000618
22	Isoc1	Isochorismatase domain-containing protein 1	2,25	0,056079	N.A	N.A
23	Igfbp5	Insulin-like growth factor-binding protein 5	2,20	0,005785	5,13	0,000618
24	Gpr180	Integral membrane protein GPR180	2,14	0,028357	0,80	0,043977
25	Osbpl10	Oxysterol-binding protein-related protein 10	2,08	0,000083	N.A	N.A
26	Acyp1	Acylphosphatase-1	2,02	0,029866	1,20	0,272694
27	Sult1d1	Sulfotransferase 1 family member D1	2,02	0,001639	2,38	0,000618
28	Syt7	Synaptotagmin-7	2,01	0,000264	1,84	0,000618
29	Dpy30	Protein dpy-30 homolog	1,97	0,064369	1,01	0,966752
30	Uevld	Ubiquitin-conjugating enzyme E2 variant 3	1,96	0,060962	0,92	0,784857
31	Zdhhc2	Palmitoyltransferase ZDHHC2	1,96	0,001802	1,23	0,048838
32	Krt19	Keratin, type I cytoskeletal 19	1,91	0,073123	0,44	0,012744
33	Ces2c	Acylcarnitine hydrolase	1,90	0,050217	N.A	N.A
34	S100a1	Protein S100-A1	1,89	0,002433	2,03	0,000618
35	Sumo1	Small ubiquitin-related modifier 1	1,89	0,025861	1,13	0,424157

Top 35 most downregulated proteins and corresponding genes by BMP2:

	Gene name	Protein name	Abundance protein Ratio: (BMP2) / (Control)	Abundance protein Ratio Adj. P-Value: (BMP2) / (Control)	Abundance mRNA Ratio: (BMP2) / (Control)	Abundance mRNA Ratio Adj. P-Value: (BMP2) / (Control)
1	Stmn1	Stathmin	0,24	0,000052	0,03	0,198626
2	C1qa	Complement C1q subcomponent subunit A	0,30	0,000045	0,02	0,000618
3	Ppp4r4	Serine/threonine-protein phosphatase 4 reg. subunit 4	0,39	0,007247	0,51	0,000618
4	Vgf	Neurosecretory protein VGF	0,45	0,000007	0,06	0,000618
5	Psat1	Phosphoserine aminotransferase	0,45	0,000213	0,37	0,000618
6	Nptx2	Neuronal pentraxin-2	0,47	0,000305	0,02	0,000618
7	Eef1b	Elongation factor 1-beta	0,47	0,076116	0,93	0,647443
8	Mcm2	DNA replication licensing factor MCM2	0,47	0,000095	0,42	0,000618
9	Mcm6	DNA replication licensing factor MCM6	0,47	0,000153	0,42	0,000618
10	Eri1	3'-5' exoribonuclease 1	0,49	0,037395	0,82	0,174334
11	Nefm	Neurofilament medium polypeptide	0,49	0,000197	0,25	0,000618
12	Gcg	Pro-glucagon	0,51	0,000596	0,32	0,000620
13	Prom1	Prominin-1	0,51	0,000317	0,19	0,000618
14	Mcn3	DNA replication licensing factor MCM3	0,53	0,000420	0,13	0,000618
15	Rif1	Telomere-associated protein RIF1	0,55	0,010896	1,00	0,980331
16	Dgkg	Diacylglycerol kinase gamma	0,55	0,000732	0,47	0,000618

17	Dmd	Dystrophin	0,56	0,024898	0,61	0,007054
18	Dbn1	Drebrin	0,56	0,000064	0,44	0,000618
19	Creld2	Protein disulfide isomerase Creld2	0,56	0,001105	0,45	0,000618
20	Gpx3	Glutathione peroxidase 3	0,57	0,007145	0,30	0,000618
21	Eppk1	Epiplakin	0,57	0,000756	0,45	0,034942
22	Cgref1	Cell growth regulator with EF hand domain protein 1	0,58	0,000560	0,55	0,836251
23	Rps25	40S ribosomal protein S25	0,59	0,002133	1,53	0,269735
24	Dync1i1	Cytoplasmic dynein 1 intermediate chain 1	0,60	0,000162	0,44	0,000618
25	Ap1s1	AP-1 complex subunit sigma-1A	0,60	0,000025	0,44	0,000618
26	Nudt7	Peroxisomal coenzyme A diphosphatase NUDT7	0,60	0,000271	0,87	0,411039
27	Tmem165	Transmembrane protein 165	0,60	0,004953	0,72	0,001174
28	Ephx1	Epoxide hydrolase 1	0,61	0,000104	0,76	0,017847
29	Rassf2	Ras association domain-containing protein 2	0,61	0,001264	0,26	0,000618
30	Erich5	Glutamate-rich protein 5	0,61	0,000294	0,53	0,062129
31	Spock1	Testican-1	0,61	0,016193	0,46	0,000618
32	Enpp2	Ectonucleotide phosphodiesterase family member 2	0,62	0,000153	0,34	0,000618
33	Sst	Somatostatin	0,63	0,075366	0,37	0,000618
34	Oat	Ornithine aminotransferase, mitochondrial	0,63	0,000717	0,52	0,000618
35	Rcn1	Reticulocalbin-1	0,64	0,000089	0,52	0,000618

Figures

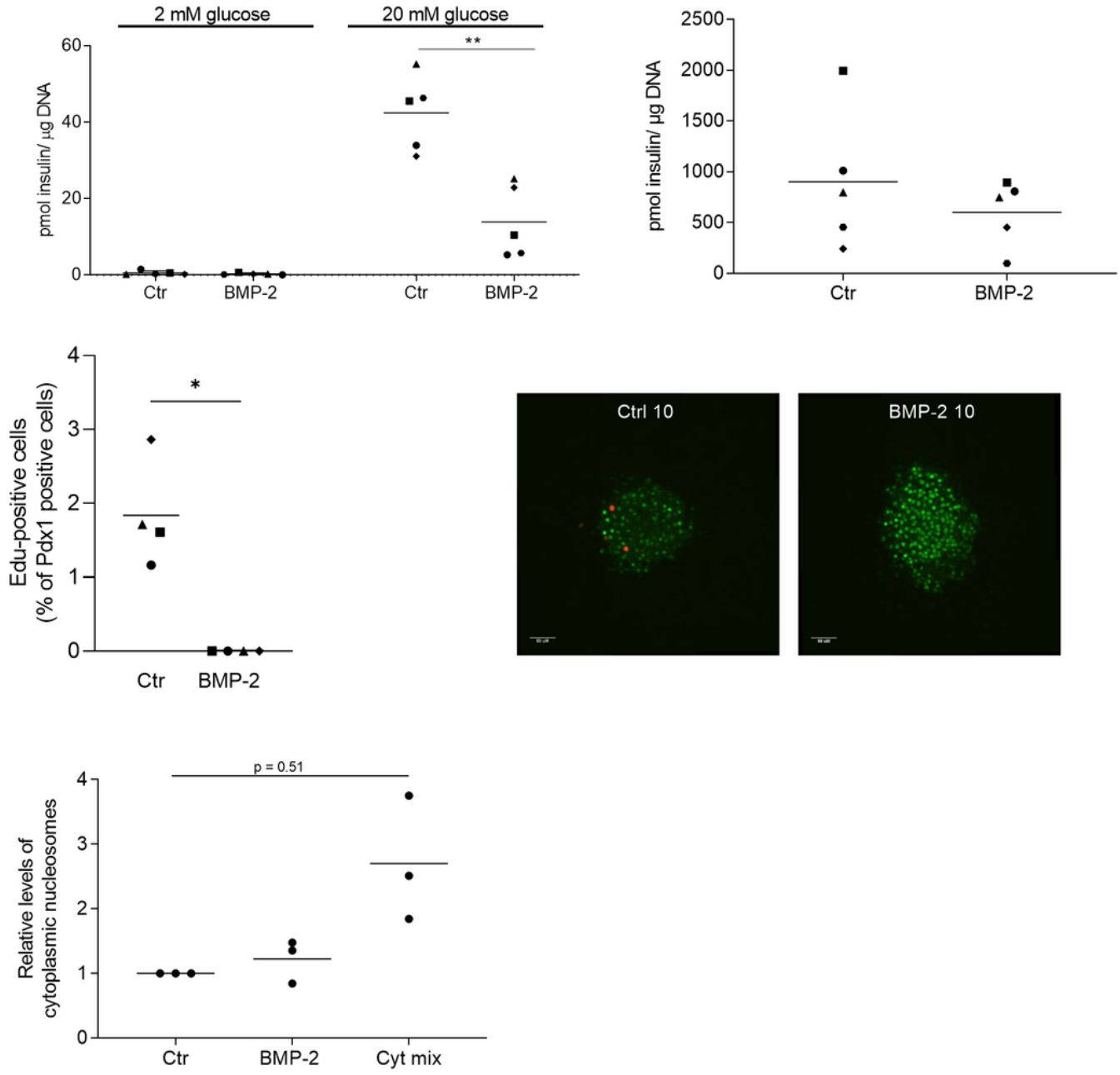

Figure 1

BMP-2 induced beta cell dysfunction and inhibition of proliferation

Mouse islets were exposed to BMP-2 (50 ng/ml) for 10 days or left non-exposed. (A) Insulin secretion was measured by static batch incubations for 30 min in response to 2 mmol/l glucose followed by 20 mmol/l and normalized to DNA content. Data are shown as means N =5, **p<0.01 2-sided paired t-test vs. ctr. (B) Total insulin content was measured post-GSIS. Data are shown as means for N =5, 2-sided t-test vs ctr. (C) Beta cell proliferation was examined in whole mouse islets exposed to BMP-2 for 10 days. Proliferation was determined by immunocytochemical staining for Pdx-1 and Click-iT detection of EdU. Results are shown as percentage of proliferating Pdx-1 positive cells. Data are shown as means for N=4, *p<0.05, 2-sided paired t-test vs. ctr. (D) Immunocytochemical and Click-iT staining of whole mouse islets. Cells were stained for Pdx-1 (green) and EdU (red). Data shown is representative. (E) Apoptosis was measured by cytoplasmic nucleosome levels in lysates from mouse islets exposed as described above. Two day stimulation with a cytokine mix of IL-1β (300 pg/ml) and IFN-γ (10 ng/ml) served as positive control for induction of apoptosis. Data are shown as means for N=3, 2-sided paired t-test vs ctr.

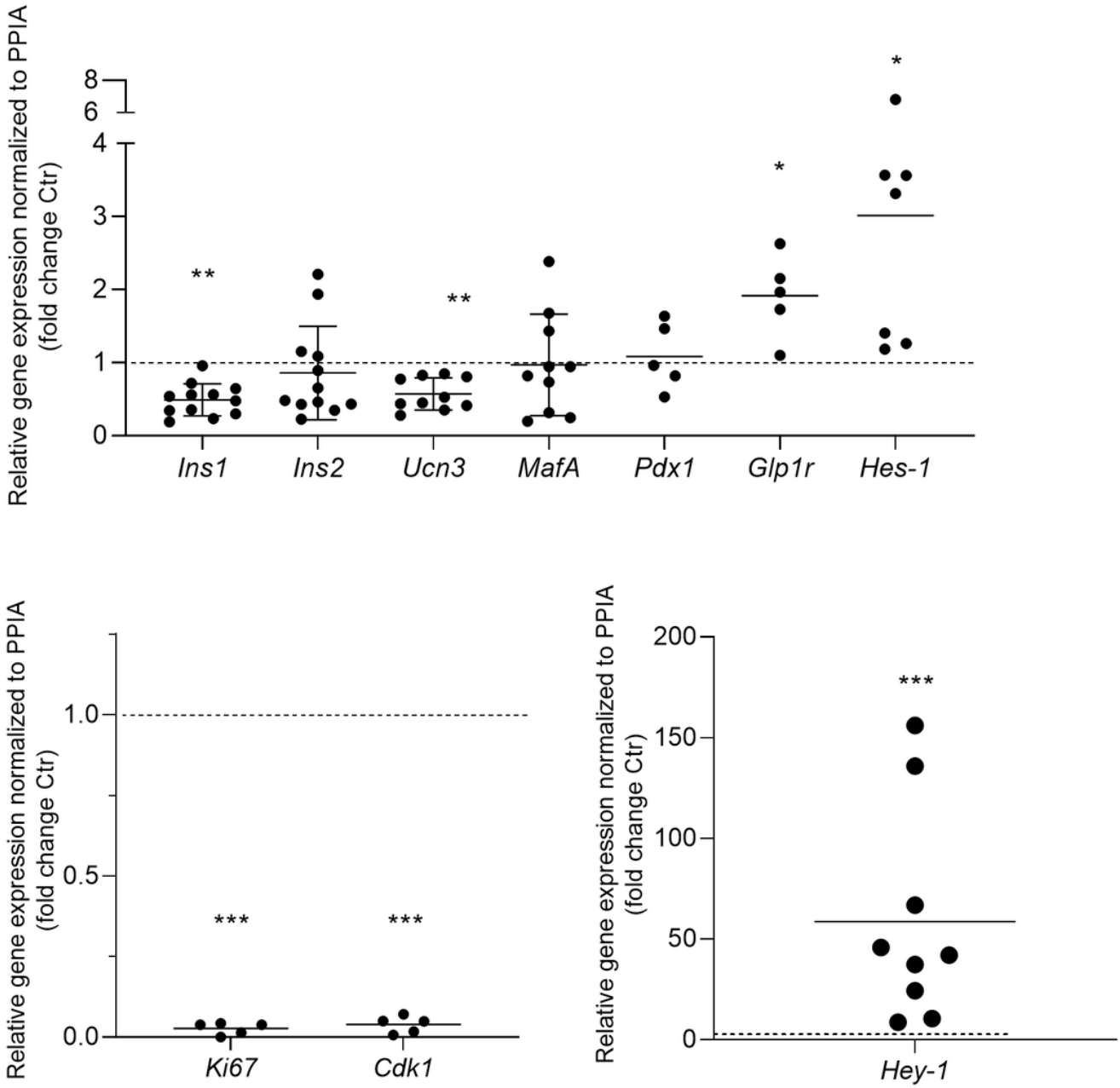

Figure 2

BMP-2 induced changes of key beta cell gene expression

Mouse islets were exposed to of BMP-2 (50 ng/ml) or left non-exposed for 10 days. Relative mRNA expression of (A) *Ins1*, *Ins2*, *Ucn3, MafA, Pdx1, Glp1r* and *Hes-1*, N=5-12 (B) *Ki67* and *Cdk1*, N=5 and (C) *Hey-1*, N=9 were analyzed using real-time PCR. Expression levels are normalized to control *Ppia*and Ctr data was set to 1 represented by the dotted horizontal line. Data are shown as means or means ± SD. *p<0.05; **p<0.01, ***p<0.001 2-sided paired t-test vs. ctr on log10 transformed data.

A)

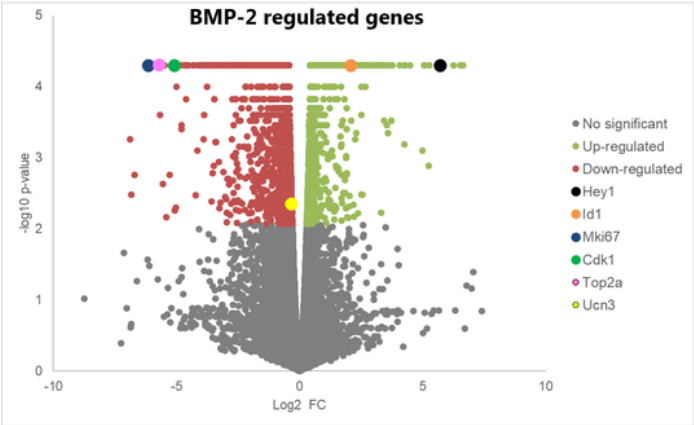

B)

Categories	Number of genes
All genes	15802 (100%)
Not significantly regulated	13099 (82.9%)
FDR <0.05 and FC> 1.5	1580 (10%)
Upregulated	612 (3.9%)
Downregulated	968 (6.1%)

C)

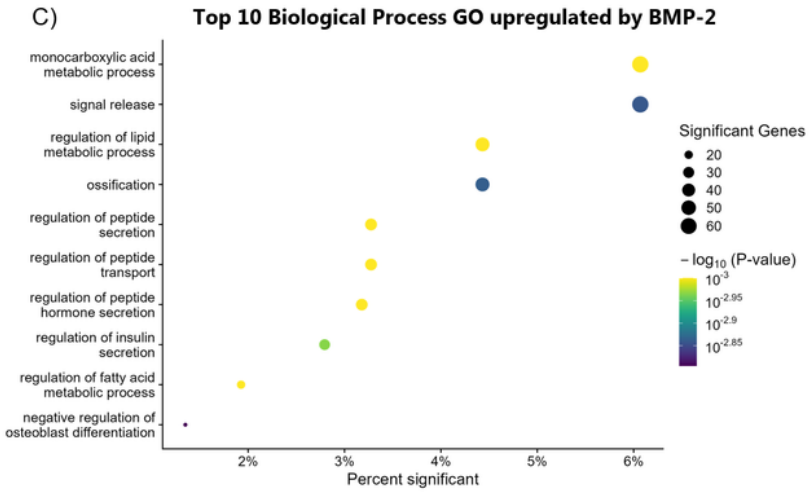

D)

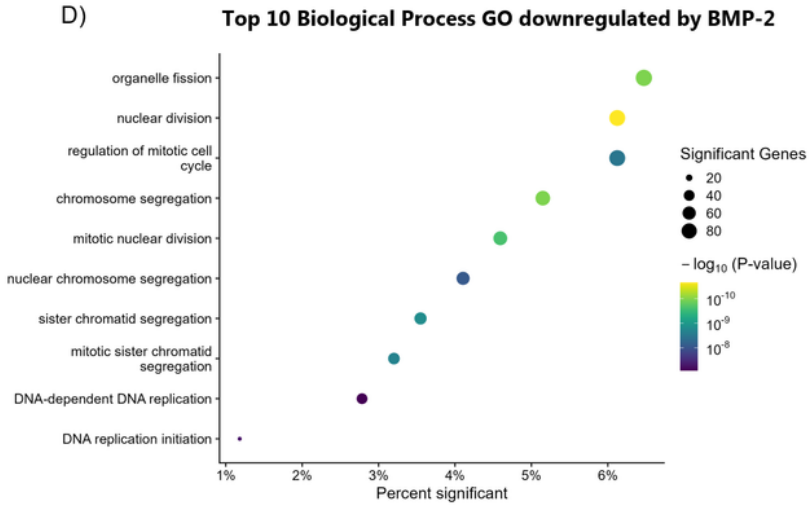

Figure 3

BMP-2 exposure affects global RNA expression

Mouse islets were exposed to BMP-2 (50 pg/ml) or left non-exposed for 10 days. (A) Volcano plot representing the differential expressed RNA's between BMP-2 vs. ctr exposed mouse islets. X-axis: log2 gene expression fold change, Y-axis: -log10 p-value. Each dot represent an individual RNA. Grey: not

significantly regulated genes, green: FDR<0.05 upregulated genes and red FDR<0.05 downregulated genes. Selected regulated genes by BMP-2 are marked (B) Table showing the summary of genes regulated by BMP-2. (C and D). Top 10 most significant enriched biological processes GO of BMP-2 upregulated and downregulated genes, respectively. X-axis: Percent of genes in the GO significantly regulated by BMP-2. Circle size: Number of significant BMP-2 regulated genes in the GO.

A)

Categories	Number of proteins
Proteins > 2 peptides	4533 (100%)
Significantly regulated	381 (8.4%)
Up-regulated	241 (5.3%)
Down-regulated	140 (3.1%)

B)

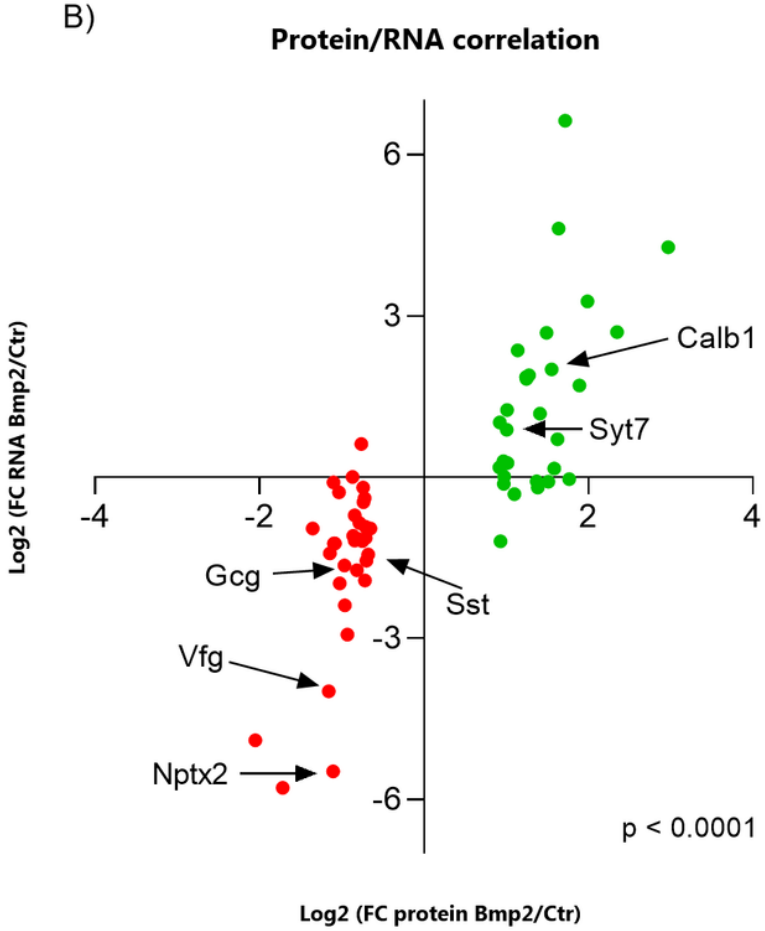

Figure 4

BMP-2 regulated gene expression correlates with protein expression

Mouse islets were exposed to BMP-2 (50 pg/ml) or left non-exposed for 10 days. Mass spectrometry was performed on extracts and (A) show significantly regulated (up or down) proteins (proteins > 2 peptides, FDR < 0.05, FC > 0.3)) in BMP-2 exposed vs. ctr islets, N=5. B) Correlation plot of Protein vs. RNA regulated by BMP-2. X-axis: Log2 (FC protein BMP-2/ctr), y-axis: Log2 (FC RNA BMP-2/ctr). Top 35 significantly up- and downregulated proteins are shown. Grey dots represent proteins where the corresponding mRNA was not significantly regulated by BMP-2. Green dots represent proteins where the corresponding mRNA was significantly upregulated by BMP-2 and red dots represent proteins where the corresponding mRNA Spearman correlation test *** p<0.0001.

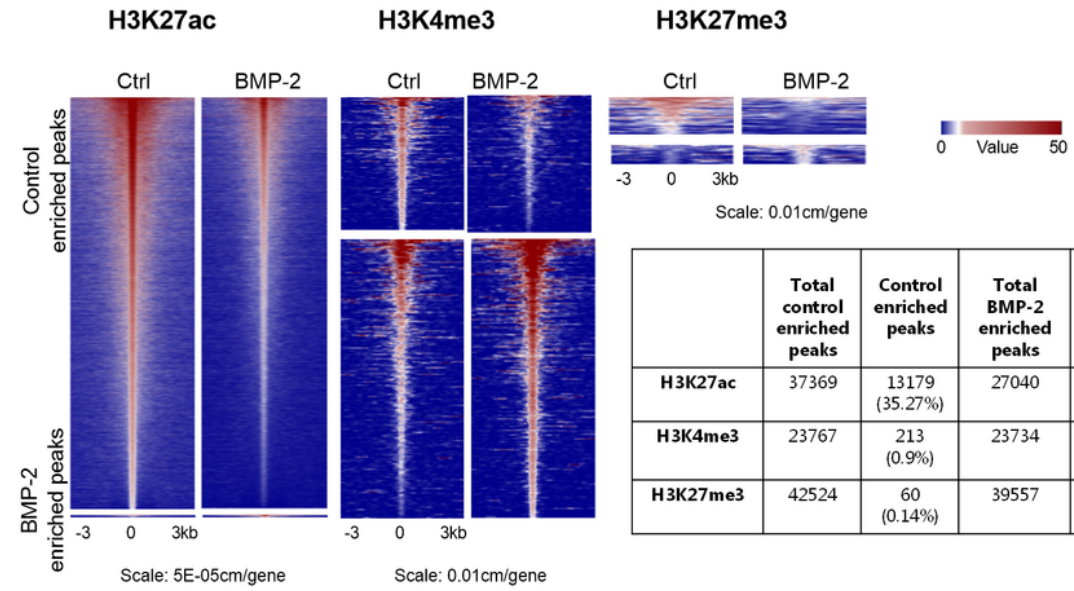

	Total control enriched peaks	Control enriched peaks	Total BMP-2 enriched peaks	BMP-2 enriched peaks
H3K27ac	37369	13179 (35.27%)	27040	432 (1.6%)
H3K4me3	23767	213 (0.9%)	23734	449 (1.89%)
H3K27me3	42524	60 (0.14%)	39557	31 (0.08%)

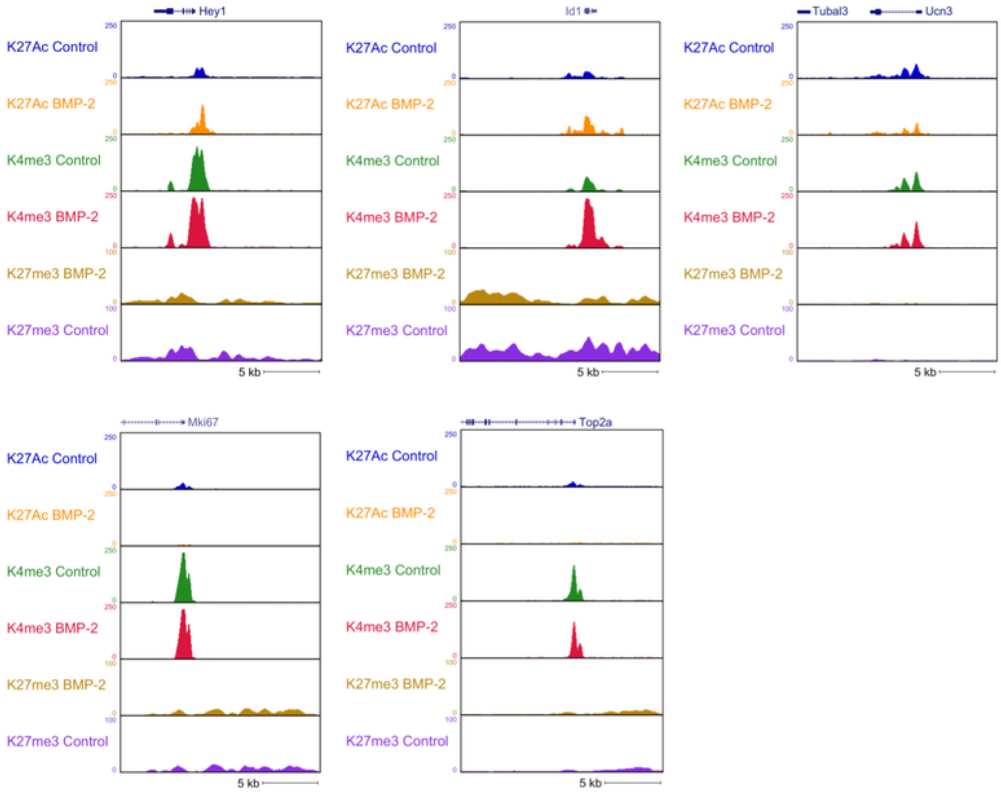

Figure 5

BMP-2 regulation of histone modifications

Analysis of chromatin histone modification in mouse islets exposed to BMP-2 (50 pg/ml) or left non-exposed for 10 days. Heat map of (A) H3K27 acetylation, (B) H3K4 tri-methylation and (C) H3K27 tri-methylation from Ctr (left) and BMP-2 exposed islets (right) from -3 kb to +3kb surrounding the center of

the peak. Each horizontal line represents a single histone 3 binding site (peak) and the color scale indicates the H3K27ac, H3K4me3 and H3K27me3 ChIP-seq tags per bp, respectively. H3K27ac scale is 5E-5 cm per peak while for H3K4me3 and H3K27me3 the scale is 0.01cm per peak. Upper panel: control enriched peaks (downregulated by BMP-2). Lower panel: BMP-2 enriched peaks (upregulated by BMP-2). (D) Table showing the summary of the number of peaks regulated by BMP-2. (E) Genome browser snapshot of ChIP-seq for selected genes; *Hey-1, Id1, Ucn3, Ki67* and *Top2a* for the 3 histone modifications (H3K27ac, H3K4me3, and H3K27me3) from ctr and BMP-2 exposed islets.

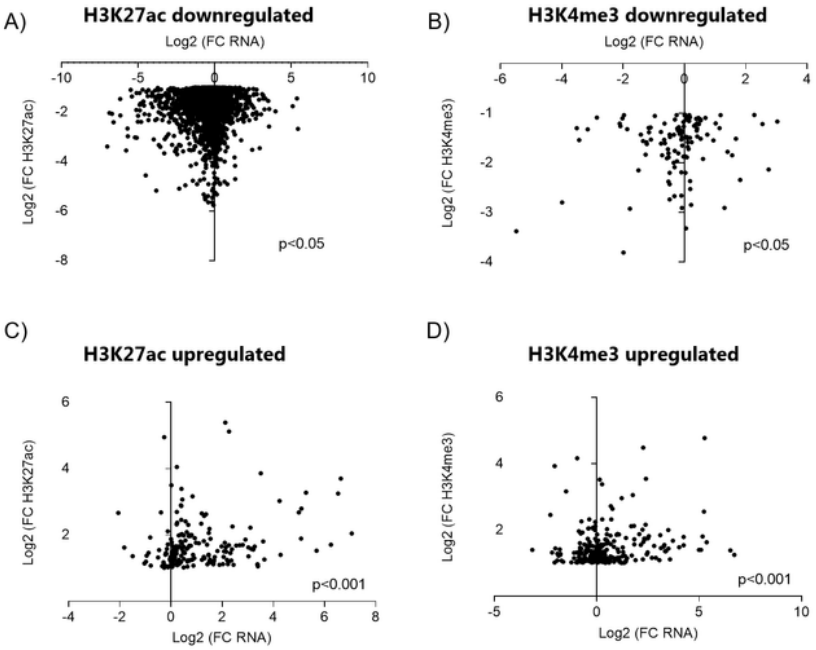

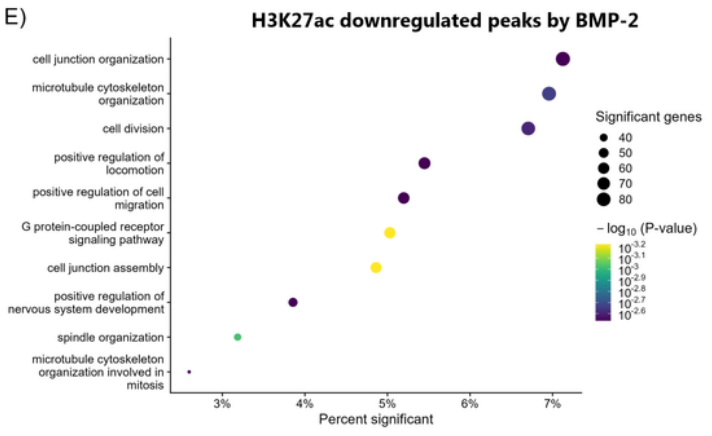

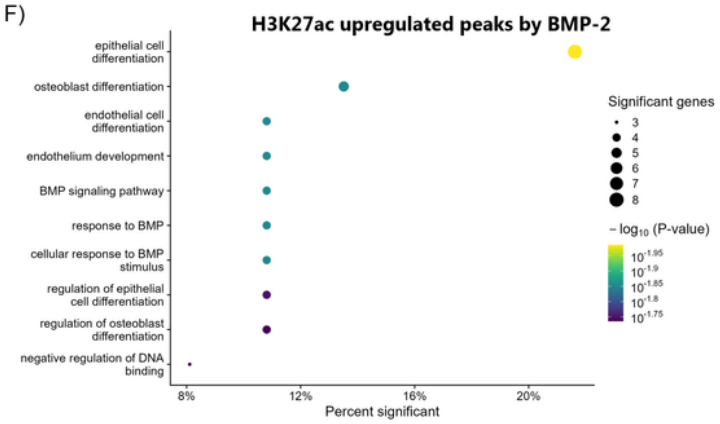

Figure 6

BMP-2 induced changes in RNA expression are associated with changes in histone modifications

Graph showing the correlation between RNA fold-change and (A) H3K27ac Ctr enriched peaks (B) H3K4me3 Ctr enriched peaks (C) H3K27ac BMP-2 enriched peaks (D) H3K4me3 BMP-2 enriched peaks. X-axis: Log2 (FC RNA) Y-axis: Log2 (FC histone modification). *p<0.05, ***p<0.001 Spearman correlation test. (E) Biological process GO analysis on H3K27ac downregulated peaks associated to TSS of genes (F) Biological process GO on H3K27ac BMP-2 upregulated peaks associated to TSS of genes. X-axis: Percent of genes in the GO with a differential peak associated to TSS. Circle: Number of genes in the GO with a BMP-2 regulated differential peak associated to their TSS.

A)

Rank	Name	P-value	% motifs for control-enriched peaks	% motifs for background enriched peaks
1	**NeuroD1(bHLH)**	**1.00E-14**	**14.16**	**9.99**
2	NeuroG2(bHLH)	1.00E-13	23.73	13.87
3	Atoh1 (bHLH)	1.00E-13	18.6	22.08

B)

	Number of binding sites
Shared binding sites	11053
Non-regulated binding sites	8641 (78%)
BMP-2 increased binding sites	73 (1%)
BMP-2 decreased binding sites	2336 (21%)

C)

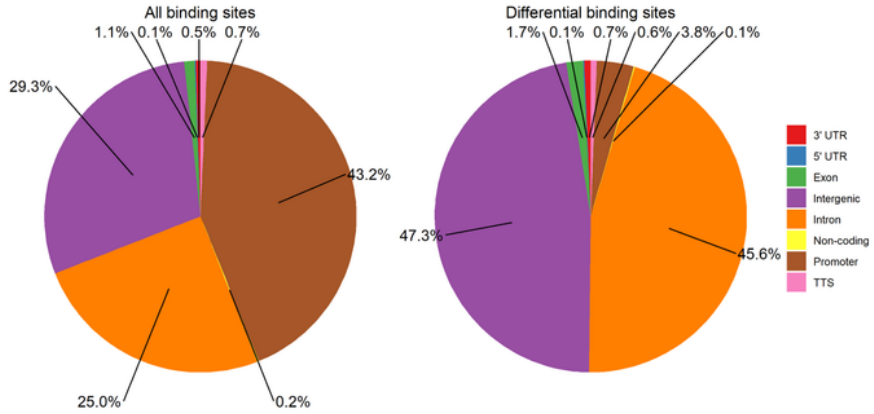

D)

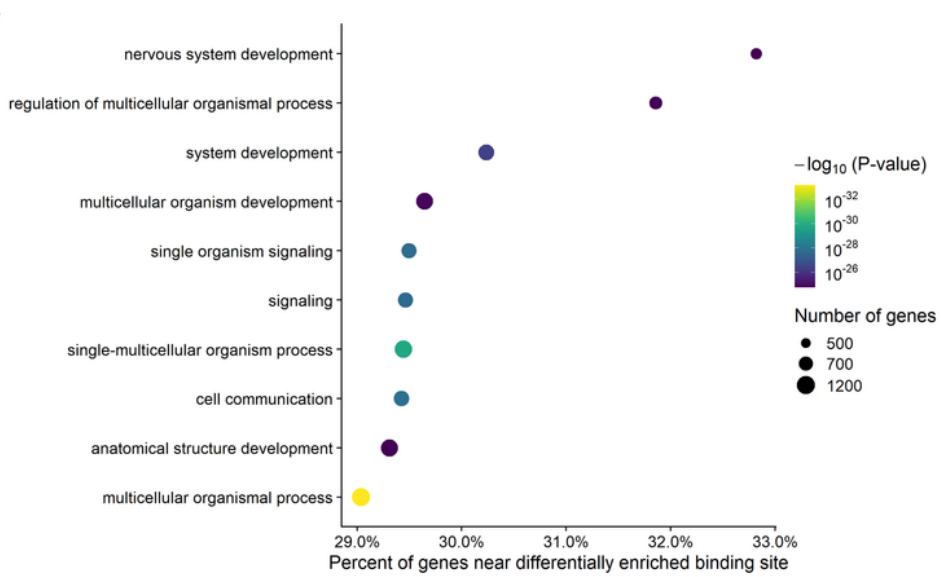

Figure 7

BMP-2 induced regulation of NeuroD1 chromatin binding

(A) Table depicting the top three enriched motifs in H3K27ac Control enriched (downregulated by BMP-2) peaks. (B) ChIP analysis showing the number of NeuroD1binding sites (peaks) upregulated and downregulated by BMP-2. (C) Distribution of NeuroD1occupied binding sites in the genome and

differential NeuroD1 binding sites in response to BMP-2. (D) Biological Processes GO analysis on BMP-2 downregulated NeuroD1 binding sites. X-axis: Percent of all genes in GO, that are near a differentially enriched binding site. Circle: Number of genes in the GO close to a differentially enriched binding site.

Supplementary Files

This is a list of supplementary files associated with this preprint. Click to download.

- Supplementarydatasheets1to20.xlsx
- Suplementaryfigures.pptx